

Photoacoustic endoscopy

Joon-Mo Yang,¹ Konstantin Maslov,¹ Hao-Chung Yang,² Qifa Zhou,² K. Kirk Shung,² and Lihong V. Wang^{1,*}

¹Department of Biomedical Engineering, Optical Imaging Laboratory, Washington University in St. Louis, Campus Box 1097, One Brookings Drive, St. Louis, Missouri 63130-4899, USA

²Resource Center for Medical Ultrasonic Transducer Technology, Department of Biomedical Engineering, University of Southern California, 1042 Downey Way, DRB 136, Los Angeles, California 90089-1111, USA

*Corresponding author: lhwang@biomed.wustl.edu

Received March 11, 2009; accepted April 3, 2009;
posted April 22, 2009 (Doc. ID 108687); published May 14, 2009

We have developed photoacoustic endoscopy with a miniaturized imaging probe. A light-guiding optical fiber, an ultrasonic sensor, and a mechanical scanning unit are integrated to enable circumferential sector scanning, which produces B-scan images. Biological tissues, including the gastrointestinal tract of a rat, have been imaged *ex vivo* or *in situ*. © 2009 Optical Society of America
OCIS codes: 170.3880, 170.5120, 180.5810.

Photoacoustic tomography has great potential for *in vivo* medical applications, because it is safe and has a high ratio of imaging depth to resolution [1–4]. It provides image information by detecting ultrasonic waves generated by absorbed energy impulses, typically laser pulses. Its deep imaging capability is attributed to its energy delivery mechanism, which uses diffused light that can penetrate up to several centimeters into soft tissue. Unfortunately, at large depths, imaging resolution can be inadequate. In such cases, the photoacoustic probe must be positioned close to the area of interest by means of endoscopy.

Other optical imaging modalities, such as optical coherence tomography (OCT) and confocal microscopy, have already shown their endoscopic potential within penetrations limited by the transport mean-free path (~ 1 mm in the skin) [5–7]; consequently, much interest has developed in the endoscopic embodiment of photoacoustic imaging. A photoacoustic endoscopic probe for 1D sensing was reported by Viator *et al.* [8] in 2001, and a more recent study [9] has presented photoacoustic images of a rabbit's blood vessels *ex vivo*, utilizing an intravascular ultrasound probe. The latter system, however, was not yet truly endoscopic, because it used external light illumination.

A photoacoustic endoscopic system has to deliver light pulses, detect ultrasonic waves, and perform area or line scanning at the tip of a small probe. A flexible-shaft-based mechanical scanning mechanism can potentially be used for the scanning method, as is done in endoscopic ultrasonography [10] and OCT [5,6]. However, unlike the thin single-mode fibers that are used in endoscopic OCT systems, the relatively thick multimode optical fibers used in photoacoustic endoscopy cannot be easily bent and rotated along with the flexible shaft. To avoid this technical issue, in this study we implement a photoacoustic endoscopic probe that combines light delivery, acoustic sensing, and mechanical scanning in one small unit placed at the distal end of the endoscope.

Figure 1 shows (a) a schematic and (b) a photograph of the distal end of our photoacoustic endo-

scopic probe. In the probe, a light-guiding optical fiber (0.22 NA, 365 μm core diameter), a single-element ultrasonic transducer (LiNbO₃, 43 MHz, 2.0 mm aperture, unfocused), and a mechanical micromotor are placed into a stainless steel tube. Laser pulses from a diode-pumped, solid-state, Nd:YLF-pumped dye laser (Cobra HRR, Sirah, 7 ns pulse duration) are guided by the optical fiber and emitted through a central hole (0.5 mm diameter) in the transducer. Circumferential sector scanning (B scan) is accomplished by rotating a mirror (3.0 mm diameter, protected aluminum on glass substrate, with the reflection surface at 45° to the probe's axis). The mirror—driven by a 1.5 mm diameter, 12.0-mm-long geared micromotor (gear ratio, 254:1; Namiki Precision Inc.)—steers both the light beam from the optical fiber to the tissue and the acoustic wave from the tissue to the transducer. Because water and glass have a large ratio of sound-propagation speeds (1.5/5.1, longitudinal wave; 1.5/3.3, shear wave), the scanning mirror exhibits total internal reflection within the acceptance angles of the ultrasonic transducer and inserts no additional propagation losses into the ultrasonic detection. The scanning-mirror system replaces the conventional flexible shaft-based

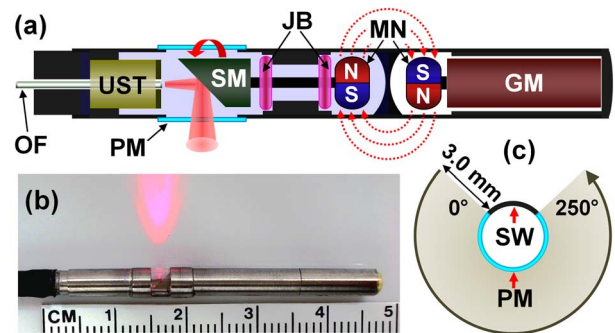


Fig. 1. (Color online) (a) Schematic of the photoacoustic endoscopic probe: GM, geared micromotor; JB, jewel bearings; MN, magnets; OF, optical fiber; PM, plastic membrane (imaging window); SM, scanning mirror; UST, ultrasonic transducer. (b) Photograph of the probe. (c) Field of view: SW, stainless-steel wall (blocked zone, 110°); PM, plastic membrane (imaging zone, 250°).

mechanical scanning, enabling circumferential B scanning without moving other illumination optics and the ultrasonic sensor.

The optical fiber, the transducer's signal wires, and the micromotor's wires are encapsulated in the flexible endoscope body. The implemented probe diameter, 4.2 mm, is currently limited by the transducer size, which can be further reduced. The mirror's rotational speed is kept constant at 2.6 Hz. To provide a matching medium for acoustic wave propagation, the transducer and scanning mirror's housing space is filled with deionized water and sealed with a 50- μm -thick low-density polyethylene (LDPE) membrane. The micromotor is isolated from the water, and the torque required for the mirror rotation is transferred through a magnetic coupling mechanism.

As shown in Fig. 1(c), the field of view is a ring partially blocked by the stainless-steel housing bridge. For each circular B-scan, 254 time-resolved photoacoustic signals (A-lines) are recorded, leading to an angular step size of $360^\circ/254=1.42^\circ$. However, 76 A-lines, corresponding to the 110° stainless-steel sector, are blocked. The maximum radial imaging depth, 3.0 mm, is determined by the 400 time points sampled at 200 MHz by a 12-bit data-acquisition card, while the speed of sound is assumed to be 1.5 mm/s. The 570 nm laser beam diverges with a half angle of 9.6° from the optical fiber and illuminates tissue over a spot of 1.55 mm in diameter at a surface fluence of $17 \text{ mJ}/\text{cm}^2$, which is within the American National Standards Institute safety limit of $20 \text{ mJ}/\text{cm}^2$ [11]. The electric signal from the transducer is transmitted by a microcoaxial cable (50 Ω ; 0.44 mm diameter, Hitachi Cable Manchester) and amplified by 48 dB through two amplifiers (ZFL-500LN+, Mini-Circuits). To minimize noise, we apply a digital bandpass filter (23–63 MHz) to the signal. In all photoacoustic images, the pixel intensity corresponds to the signal amplitude calculated via Hilbert transformation of the time-domain signals.

To determine the performance of the system, we imaged a 6 μm diameter carbon fiber in clear (deionized water) and turbid media (0.25% Intralipid solution; $\mu'_s \approx 3.5 \text{ cm}^{-1}$); the results are shown in Fig. 2. Because the central acoustic wavelength of the transducer is much longer than the carbon-fiber diameter, the carbon fiber can be treated as an ideal line target. In Fig. 2(a), we present a typical A-line signal acquired from the carbon fiber, along with the amplitude of its Hilbert transform (envelope). From the envelope, we determined the radial resolution based on the -6 dB width and also determined the signal-to-noise ratio (SNR) as a ratio of the peak signal magnitude to the noise fluctuation (standard deviation). Figure 2(b) shows the carbon fiber's transverse (angular or tangential) point spread function (PSF). The carbon fiber's photoacoustic B-scan images are plotted in Cartesian and polar coordinate formats in (c) and (d), respectively. In Figs. 2(e)–2(g), the system's SNR, radial resolution, and transverse resolution are plotted versus the target's position measured from the plastic membrane surface, where 30 B-scan images were averaged. In Fig. 2(e), the clear medium's

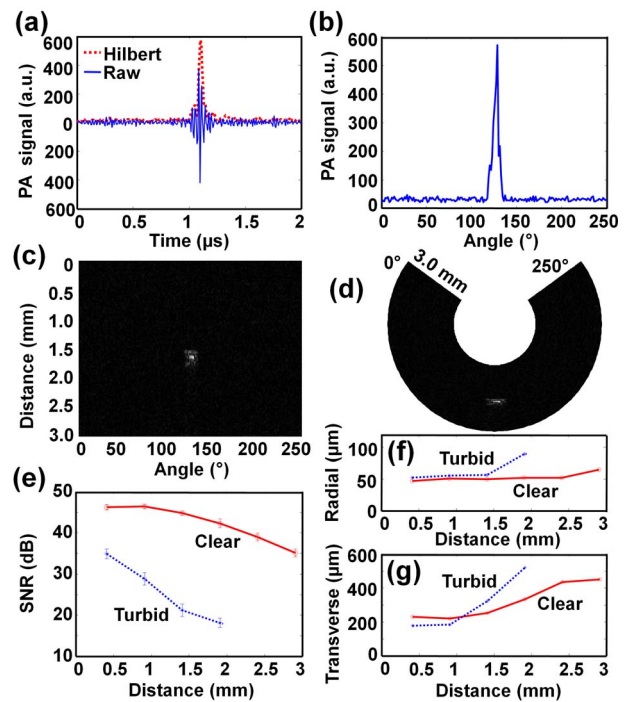


Fig. 2. (Color online) (a) Typical photoacoustic (PA) A-line of the carbon fiber: raw data and amplitude of the Hilbert-transform. (b) Transverse PSF for the carbon fiber. (c) Photoacoustic image of a carbon fiber (6 μm in diameter): Cartesian coordinate representation. (d) Polar-coordinate representation of image (c). (e) SNR versus target distance. (f) Radial resolution versus target distance. (g) Transverse resolution versus target distance.

SNR equals 46 dB near the probe's surface but decreases to 35 dB at a depth of ~ 2.9 mm. The turbid medium's SNR is lower than that of the clear medium, decreasing from 35 to 18 dB within a 1.9 mm depth owing to faster optical fluence decay. As seen in Fig. 2(f), the radial resolution in the clear medium slowly worsens with target distance, from 47 μm to 65 μm . The turbid medium's resolution ranges from 52 μm near the probe's surface to 89 μm at the 1.9 mm depth. In Fig. 2(g), the transverse resolution in the clear medium degrades gradually from 230 μm to 450 μm with increasing target distance, but that in the turbid medium does so from 177 μm to 520 μm .

We demonstrate our system's imaging ability by imaging three tissue samples of a rat (Sprague Dawley rats; ~ 250 g; Harlan National Customer Service Center) (Fig. 3). The animal was sacrificed first by an overdose of pentobarbital (120 mg/kg, IP), and the abdomen was depilated by a commercial hair-removing lotion. All experimental animal procedures were carried out in compliance with the guidelines of the U.S. National Institutes of Health. The laboratory animal protocol for this work was approved by the Animal Study Committee of Washington University in St. Louis, Missouri.

First, we imaged the rat's abdominal surface *in situ*, as shown in Fig. 3(a). The dashed arrow in the photograph indicates the scanning direction and range. The corresponding photoacoustic B-scan image is presented in Fig. 3(b). In the photoacoustic im-

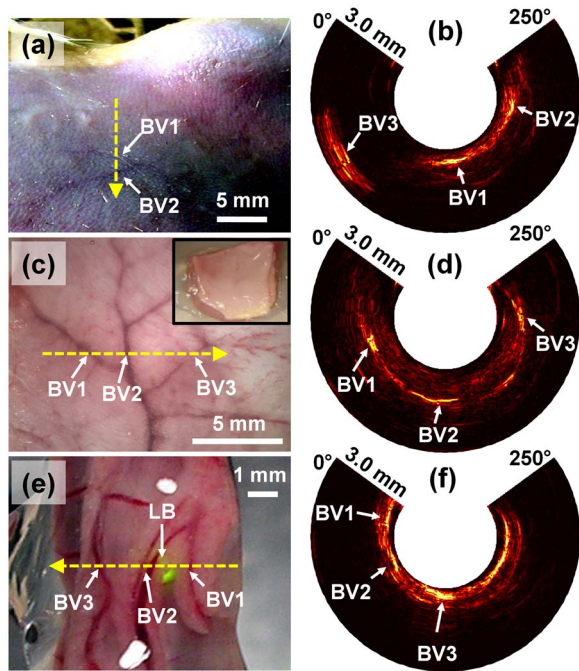


Fig. 3. (Color online) (a) Photograph of the rat's abdominal surface. (b) Photoacoustic (PA) B-scan image of the tissue shown in (a). (c) Photograph of the rat's abdominal tissue segment (inner surface). The inset shows the whole sample from the outside. (d) PA image of the tissue shown in (c). (e) Photograph of the intact large intestinal tract, into which the endoscope was inserted. (f) PA image of the tissue shown in (e) from inside the intestine. BV, blood vessel; LB, laser beam (570 nm). Dashed arrow, scanning direction and range.

age, two blood vessels (BV1, BV2) are seen with strong signals at a depth of ~ 0.5 mm, and their positions match the blood vessel positions in the photograph well. In the photoacoustic image, another blood vessel (BV3) at a depth of ~ 2.5 mm is seen with a strong signal; however, it is invisible in the photograph, which demonstrates our endoscope's deep imaging capability in highly scattering skin tissue. Second, to demonstrate the blood-vessel mapping capability, we imaged an excised abdominal tissue segment of the rat *ex vivo* through its inner surface, as shown in Fig. 3(c). The inset at the upper right corner shows the entire sample from outside. In the photoacoustic B-scan image presented in Fig. 3(d), three blood vessels appear at a depth of 1.0 mm, corresponding well with those in the photograph. Third, to show the endoscopic potential, we imaged an intact large intestinal tract of the rat *ex vivo*, as shown in Fig. 3(e). The endoscopic probe was inserted into the intestinal tract, where the spot just below the dashed arrow indicates the laser beam's position. In the photograph, we can see three blood vessels across the scanning line; all three are mapped well in the photoacoustic image [Fig. 3(f)]. From the photoacoustic image, the intestinal wall's thickness is estimated to be ~ 1.0 mm.

In conclusion, we have presented the concept of and implemented a system for photoacoustic endoscopy and demonstrated the feasibility of our scanning-mirror-based system through *ex vivo* imaging experiments. The scanning mirror that deflects both light and sound makes the system simple, stable, and flexible. In our prototype photoacoustic endoscope, the angular scanning range was restricted by the stainless-steel wall of the probe, which, however, can be replaced with an optically and acoustically transparent plastic material, such as LDPE; therefore, full-ring views are attainable. The lateral resolution of the system can be significantly improved by focusing either the ultrasonic transducer or the scanning mirror, or both. Photoacoustic endoscopy is expected to be complementary to other forms of endoscopy, because it is exquisitely sensitive to optical absorption and able to reach depths beyond the optical-transport mean-free path.

This research was supported by the U.S. National Institutes of Health (NIH) grants R01 NS46214 (BRP), R01 EB000712, R01 EB008085, and U54 CA136398 (Network for Translational Research). L. W. has a financial interest in Endra, Inc., which, however, did not support this work. J. M. Y. was supported in part by a Korea Research Foundation (KRF) grant funded by the Korean Government (KRF-2007-357-C00039).

References

1. L. V. Wang, ed., *Photoacoustic Imaging and Spectroscopy* (Taylor & Francis/CRC Press, 2009).
2. A. A. Oraevsky and A. A. Karabutov, in *Biomedical Photonics Handbook*, T. Vo-Dinh, ed. (CRC Press, 2003), Vol. PM125, Chap. 34.
3. K. Maslov, G. Stoica, and L. V. Wang, *Opt. Lett.* **30**, 625 (2005).
4. H. F. Zhang, K. Maslov, G. Stoica, and L. V. Wang, *Nat. Biotechnol.* **24**, 848 (2006).
5. G. J. Tearney, S. A. Boppart, B. E. Bouma, M. E. Brezinski, N. J. Weissman, J. F. Southern, and J. G. Fujimoto, *Opt. Lett.* **21**, 543 (1996).
6. S. H. Yun, G. J. Tearney, B. J. Vakoc, M. Shishkov, W. Y. Oh, A. Desjardins, R. Chan, M. Suter, J. Evans, I. K. Jang, N. S. Nishioka, J. F. de Boer, and B. E. Bouma, *Nat. Med.* **12**, 1429 (2006).
7. R. Kiesslich, J. Burg, M. Vieth, J. Gnaendiger, M. Enders, P. Delaney, A. Polglase, W. McLaren, D. Janell, S. Thomas, B. Nafe, P. R. Galle, and M. F. Neurath, *Gastroenterol.* **127**, 706 (2004).
8. J. A. Viator, G. Paltauf, S. L. Jacques, and S. A. Prahl, *Proc. SPIE* **4256**, 16 (2001).
9. S. Sethuraman, S. R. Aglyamov, J. H. Amirian, R. W. Smalling, and S. Y. Emelianov, *IEEE Trans. Ultrason. Ferroelectr. Freq. Control* **54**, 978 (2007).
10. J. Menzel and W. Domschke, *Am. J. Gastroenterol.* **95**, 605 (2000).
11. Laser Institute of America, *American National Standard for the Safe Use of Lasers*, ANSI Z136.1-2000 (American National Standards Institute, Inc., 2000).